Agricultural and Forest Meteorology 249 (2018) 44–56

Contents lists available at ScienceDirect

Agricultural and Forest Meteorology

journal homepage: www.elsevier.com/locate/agrformet

A steady-state approximation approach to simulate seasonal leaf dynamics of deciduous broadleaf forests via climate variables

Qinchuan Xin[a,*], Yongjiu Dai[b,*], Xia Li[a], Xiaoping Liu[a], Peng Gong[c], Andrew D. Richardson[d,e]

[a] Guangdong Key Laboratory for Urbanization and Geo-simulation, Sun Yat-sen University, Guangzhou 510275, China
[b] School of Atmospheric Sciences, Sun Yat-sen University, Guangzhou 510275, China
[c] Department of Earth System Science, Tsinghua University, Beijing 100084, China
[d] School of Informatics, Computing and Cyber Systems, Northern Arizona University, Flagstaff, AZ 86011, USA
[e] Center for Ecosystem Science and Society, Northern Arizona University, Flagstaff, AZ 86011, USA

ARTICLE INFO

Keywords:
Leaf area index
Phenology
Growing production-day
Ecosystem
Climate change

ABSTRACT

As leaves are the basic elements of plants that conduct photosynthesis and transpiration, vegetation leaf dynamics controls canopy physical and biogeochemical processes and hence largely influences the interactive exchanges of energy and materials between the land surface and the atmosphere. Given that the processes of plant leaf allocation is highly sensitive to climatological and environmental conditions, developing robust models that simulate leaf dynamics via climate variables contributes a key component to land surface models and coupled land-atmosphere models. Here we propose a new method to simulate seasonal leaf dynamics based on the idea of applying vegetation productivity as a synthesized metric to track and assess the climate suitability to plant growth over time. The method first solves two closed simultaneous equations of leaf phenology and canopy photosynthesis as modeled using the Growing Production-Day model iteratively for deriving the time series of steady-state leaf area index (LAI), and then applies the method of simple moving average to account for the time lagging of leaf allocation behind steady-state LAI. The seasonal LAI simulated using the developed method agree with field measurements from a selection of AmeriFlux sites as indicated by high coefficient of determination (R^2 = 0.801) and low root mean square error (RMSE = 0.924 m^2/m^2) and with satellite-derived data (R^2 = 0.929 and RMSE = 0.650 m^2/m^2) for the studied flux tower sites. Moreover, the proposed method is able to simulate seasonal LAI of deciduous broadleaf forests that match with satellite-derived LAI time series across the entire eastern United States. Comparative modeling studies suggest that the proposed method produces more accurate results than the method based on Growing Season Index in terms of correlation coefficients and error metrics. The developed method provides a complete solution to modeling seasonal leaf dynamics as well as canopy productivity solely using climate variables.

1. Introduction

The Earth is an integrated and complex system that consists of interrelated components, such as biosphere, atmosphere, hydrosphere, cryosphere, pedosphere, and lithosphere. As a key constituent component of the Earth system, the land surface interacts with the atmosphere by exchanging massive fluxes of energy and materials (Bonan, 2002). Terrestrial plants have considerable impacts on the climate by releasing water vapor to the atmosphere through transpiration and removing atmospheric carbon dioxide through photosynthesis (Beer et al., 2010). The climate, in turn, controls plant growth and subsequent physical and biogeochemical processes (Keenan et al., 2013; Zhu et al., 2017). Robust simulation of canopy processes and fluxes is then essential to understand the land surface-atmosphere interactions and hence global carbon cycle and water cycle of the Earth system.

One key to successful modeling of canopy exchanges between the land surface and the atmosphere is to develop and solve two simultaneous equations. Given that leaves are the basic elements of plants that conduct photosynthesis and control transpiration, the land surface models commonly use leaf area index (LAI) to characterize vegetation canopy (Clark et al., 2011; Dai et al., 2003; Oleson et al., 2013; Sellers et al., 1996), and thus the first equation is to simulate canopy fluxes such as gross primary production (GPP) and evapotranspiration given known LAI on the ground. Thanks to decades of scientific advances in land surface studies, the models that describe the first equation, despite differing from each other in terms of sophistication, have been

* Corresponding authors at: Sun Yat-Sen University, Earth and Environment Building D101, Guangzhou 510275, China.
E-mail addresses: xinqinchuan@gmail.com (Q. Xin), daiyj6@mail.sysu.edu.cn (Y. Dai).

https://doi.org/10.1016/j.agrformet.2017.11.025
Received 22 September 2017; Received in revised form 9 November 2017; Accepted 21 November 2017
Available online 24 November 2017
0168-1923/

reasonably formulated and could be generalized as follows:

$$[GPP, ET] = f(LAI, E_{1,2,...n}) \quad (1)$$

where *GPP* denotes gross primary production [gC/m^2/day], *ET* denotes evapotranspiration [W/m^2], *f* denotes a certain function with inputs in the parenthesis, *LAI* denotes leaf area index [m^2/m^2], and $E_{1,2,...n}$ denotes various environmental variables (e.g., temperature, vapor pressure deficit, photoperiod, elevation, and soil moisture).

As external environmental variables in vegetation models are typically considered as known conditions that could be obtained from observations or atmospheric circulation models, the second equation is to provide complementary LAI to the first equation by simulating the leaf dynamics solely using climate variables. Solving the second equation, as generalized as follows, essentially involves the study and modeling of vegetation phenology and its interaction with the environment:

$$LAI = f(E_{1,2,...n}) \quad (2)$$

where *LAI* denotes leaf area index [m^2/m^2], and $E_{1,2,...n}$ denotes various environmental variables.

Vegetation phenology modeling has been found highly uncertain in the land surface models and is challenging for reasons (Friedl et al., 2014; Richardson et al., 2012). While understanding the exact role of each individual climate factor in leaf allocation is needed for model developments, the climate drivers affect vegetation phenology through various physiological and biochemical processes with interrelated impacts. Moreover, the physiological processes of plant leaf allocation responds to climate variation relatively slowly, ranging from days to months, such that there is a need to account for the time lag effects by using preceding climate variables when simulating seasonal leaf dynamics. In response to climate conditions, plant species have evolved distinct canopy structures and their own strategies of leaf allocation to optimize the acquisition of natural resource (Givnish, 1986). Importantly, developing models of leaf dynamics requires recording influential climate variables and plant phenology simultaneously and continuously, while key phenophases, such as the events of leaf emergence, maturation, senescence, and dormancy, typically occur only once (or at most twice) in a year (Broich et al., 2014), making data from traditional field measurements limited, especially when taking the factors of weather conditions and equipment malfunctions into account. Fortunately, land surface observations from flux towers, automated camera networks, and remote sensing now offer opportunities for developing and validating comprehensive phenology models (Ganguly et al., 2010; Hufkens et al., 2012; Yang et al., 2013).

Typically, the models of plant phenology are developed separately from the canopy model of photosynthesis and evapotranspiration. One approach to characterize vegetation leaf dynamics is to simulate the timing of key phenophases such as spring onset and autumn senescence using climate variables (Melaas et al., 2016; Yang et al., 2012). For example, acknowledging temperature as one of the most important factors that affect biochemical reactions and hence leaf allocation, the Growing Degree Day (GDD) model accumulates daily temperatures to predict the occurrence of spring onset when heating accumulation reaches a certain heating forcing (Chuine et al., 1999). To account for the impacts of environmental drivers other than temperature, the GDD derivative models downregulate heating accumulation by adding constraint functions of different climate variables, such as chilling temperature, photoperiod, vapor pressure deficit, and soil water stress (Melaas et al., 2013; White et al., 1997; Xin et al., 2015a). Complex land surface models like the Community Land Model use a set of empirical functions to downregulate heating accumulation, thereby predicting spring onset and autumn senescence (Oleson et al., 2013). Other than predicting specific dates of key phenophases, biogeochemical models such as DeNitrification-DeComposition choose to first simulate optimal LAI time series using the GDD time series and then simulate stressed LAI time series using empirical functions derived based on other environmental factors (Li, 2000). Jolly et al. (2005) proposed the Growing Season Index (GSI), a product of three indices as derived from temperature, vapor pressure deficit, and photoperiod, respectively, to quantify the time series of vegetation greenness throughout the year. Note that GSI essentially downregulates GDD accumulations with additional considerations for evaporative demand and daylength. To sum up, while existing methods have varied degrees of success in simulating seasonal leaf dynamics of vegetation, most of them are largely empirical to date and thus have limitations in climate change studies (Arora and Boer, 2005).

Different from existing approaches, Xin (2016) developed a synthesized model that integrates the canopy model of photosynthesis and evapotranspiration for simulating vegetation phenology. The model, named as the Growing Production-Day (GPD) model, has an analogous form to the GDD model and its derivatives, but accumulates vegetation productivity instead of environmental temperature in time series. In essence, the GPD model considers plant photosynthetic productivity as the first-order control determining leaf allocation and applies the productivity of a hypothetical reference vegetation cover as a synthesized metric instead of environmental temperature to track and assess the climate suitability to plant growth over time. The timing of vegetation spring onset is then predicted as the optimal point that balances the inevitable conflict between greater productivity benefits and higher hazard damage risks underlying the plant strategy of earlier leaf allocation. The GPD model has explicit biological explanations and synthesizes all environmental factors that affect photosynthetic activities and hence vegetation phenology. Although the GPD model has shown to simulate the timing of spring onset for different biomes well, there is a need to develop further solutions for modeling the entire time series of seasonal leaf dynamics.

The goals of this study are to: 1) develop an approach to simulate seasonal leaf dynamics of vegetation, and 2) evaluate the model performance for deciduous broadleaf forests in eastern United States using field measurements and satellite data.

2. Methods and materials

2.1. A steady-state approximation approach

The physiological processes that regulate canopy photosynthesis and vegetation phenology do not respond to the climate variation instantaneously and simultaneously. The biochemical process of leaf photosynthesis usually takes one minute to reach the steady-state condition. In addition, plants open and close the stomata, numerous microscopic pores on the surfaces of leaves, to control the diffusion rates of carbon dioxide into leaves for photosynthesis. The stomatal conductance, a metric that measures the rates of carbon dioxide entering and water vapor leaving leaf stomata, usually takes several minutes to approach the steady state (Sellers et al., 1996). By comparison, the biogeochemical processes that plants allocate biomass to leaves could take up days to months under a changing climate (Zeng et al., 2013). Because vegetation phenology is typically modeled at daily or sub-daily time steps, it is then reasonable to treat plant photosynthesis as a near-instantaneous process on the daily or hourly basis, but simulate vegetation phenology as lagging behind the steady state. As such, the proposed method is to first solve the steady state of leaf dynamics and then account for the time lagging of leaf allocation behind the steady state.

Plants conduct photosynthesis and convert solar radiation into chemical energy to fuel all subsequent activities of organisms. Under the pressure of national selection, plants have evolved their strategies to compete resources such as light, water, and nutrients for photosynthesis (Eagleson, 2005; Menzel, 2002). As such, given unchanging environment conditions (i.e., limited natural resources), vegetation leaf dynamics would eventually reach a steady state if time approaches infinity, meaning that the total canopy LAI becomes unchanging as foliation balances defoliation under the competition pressures from

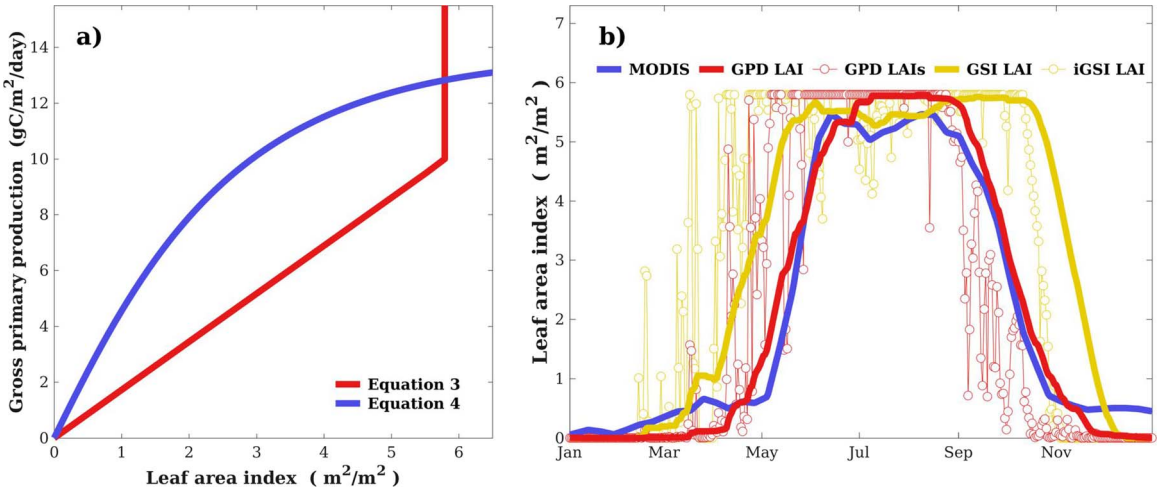

Fig. 1. Demonstrative examples of the modeling methods are shown for a) the solutions to the simultaneous equations and b) time series of satellite-based and modeled leaf area index (LAI). In the figure, GPD LAIs denotes the steady-state leaf area index derived using the growing production-day model, GPD LAI denotes the leaf area index modeled using the growing production-day model (i.e., 21-day simple moving average of GPD LAIs), iGSI LAI denotes the instantaneous leaf area index derived using the growing season index, and GSI denotes the leaf area index modeled using the growing season index (i.e., 21-day simple moving average of iGSI LAI). Climate data used in Fig. 1a were acquired on Jun 1st in 2011 at the US-Oho site (Table 2) and all data used in Fig. 1b were obtained for the entire year of 2011 at the US-Oho site.

both within and between species. In the natural environment, deciduous broadleaf forests have evolved themselves to adapt to the climates with two distinct steady states during a growing season: dormancy with leaf absence when the climate is unsuitable for plant growth and maturation with canopy closure when plant leaves reach the carrying capacity in an environment. Solving LAI at the steady state as the point that photosynthesis could sustain by using the simplest form of a linear function that meets both steady state conditions, we are able to write an equation as follows:

$$LAI_s = \min\left(\frac{GPP_s}{GPP_c} LAI_c,\ LAI_c\right) \tag{3}$$

where LAI_s denotes leaf area index at the steady state condition given fixed environmental conditions [m^2/m^2], GPP_s denote gross primary production at the steady state condition given fixed environmental conditions [$gC/m^2/day$], LAI_c denotes leaf area index at canopy closure [m^2/m^2], and GPP_c denotes mean gross primary production at canopy closure [$gC/m^2/day$].

The solution, although having a simple form, provides a key complementary equation to Eq. (1), since canopy LAI and GPP at canopy closure (LAI_c and GPP_c) can be obtained from observational data as prescribed parameters. In essence, the above equation applies the photosynthetic capacity under given environmental conditions to quantify the carrying capacities of the environment. Note that all environmental factors that influence the photosynthetic activities as quantified using the metric of steady-state gross primary production (GPP_s) would affect leaf allocations. If the overall environmental condition is not suitable for photosynthesis ($GPP_s = 0$), then there are no leaf presence for the steady state ($LAI_s = 0$), whereas total canopy LAI is capped at canopy closure. If substituting the variables of LAI_s and GPP_s into a well-developed photosynthesis model like the GPD model (see Section 2.2 for details), then we obtain another equation as follows and hence closed simultaneous equations of both Eqs. (3) and (4):

$$GPP_s = f(LAI_s, E_{1,2,\ldots n}) \tag{4}$$

where LAI_s denotes leaf area index at the steady state condition given fixed environmental conditions [m^2/m^2], GPP_s denote gross primary production at the steady state condition given fixed environmental conditions [$gC/m^2/day$], and $E_{1,2,\ldots n}$ denotes various environmental variables.

One key prerequisite to solving the simultaneous equations is that Eqs. (3) and (4) must converge. Note that Eq. (3) is a linear function and Eq. (4) is a logarithmic function passing through the origin in the space of GPP and LAI because GPP increases as LAI increases and saturates when the leaf radiation absorption saturates under given environmental conditions. Taking an example as shown in Fig. 1a, two solutions can be obtained as the crossover points of the lines of the two functions. As one of the crossover points is the origin, the needed LAI_s is then solved as the larger one. Note that because inputs to both equations are convolved and the modeling of canopy photosynthesis (i.e., Eq. (4)) often involves a complex model, the simultaneous equations of Eqs. (3) and (4) cannot be solved directly. Numerical solutions however can be obtained by the method that first gives initial LAI values and then solves for approximated values of the steady state iteratively until converging.

Once applying the steady-state method to time series observations of climate conditions, we could obtain steady-state LAI time series that tracks the climatic suitability to plant growth in a leading phase (see for an illustrative example shown in Fig. 1b). Note that the solved steady-state LAI fluctuates unrealistically as daily climate variation is high and thus there is a need to buffer single extreme events from triggering canopy changes prematurely. There are generally two methods to make the model have the ability for predicting vegetation phenology: one is to accumulate daily values and predict the timing of specific phenology events such as spring onset and autumn senescence, and another is to adopt the method of simple moving average and make predictions of the entire time series. Here we apply the second method to the preceding time series of the steady-state LAI and simulate LAI as follows:

$$LAI = SMA(LAI_s, n) \tag{5}$$

where LAI denotes leaf area index [m^2/m^2], LAI_s denotes leaf area index at the steady state condition [m^2/m^2], n denotes the number of days in the sample window, and SMA denotes the operation of simple moving average.

2.2. Modeling photosynthesis using the GPD model

Applying the steady-state approach to model LAI time series requires a robust model that simulates canopy photosynthesis, whereas canopy models with varied degrees of sophistication are available (Dai et al., 2003; Oleson et al., 2013; Running et al., 2000; Ryu et al., 2011; Sellers, 1985). Here, we apply the GPD model, a coupled model that extends our previous work (Xin et al., 2015b, 2016) and synthesizes state-of-the-art models, to simulate canopy photosynthesis. The GPD

Table 1
The generalized equations for the growing production-day model to simulate canopy photosynthesis and evapotranspiration.

model name	equations
canopy radiative transfer	$[PAR_l, R_{ln}, R_{sn}] = f(R_g, R_d, \theta, L, \Omega)$
leaf photosynthesis	$A_n = f(PAR_l, T_l, Photo, SWC, P_{atm}, g_s, c_i)$
leaf conductance	$[g_s, g_b, c_i] = f(A_n, VPD, P_{atm}, u, [CO_2])$
leaf transpiration	$[\lambda E_l, T_l] = f(R_{ln}, T_a, VPD, P_{atm}, g_s, g_b)$
soil evaporation	$\lambda E_s = f(R_{sn}, T_a, VPD, P_{atm})$

where PAR_l denotes the radiation absorbed by either sunlit or shaded leaves per leaf hemi-surface area at the photosynthetically active radiation wavelength [W m^{-2}]; R_{ln} denotes the net shortwave radiation at the leaf surface [W m^{-2}]; R_{sn} denotes the net shortwave radiation at the soil surface [W m^{-2}]; f denotes the function with input arguments in parenthesis; R_g denotes daily total incoming solar radiation at the canopy top [MJ m^{-2} day^{-1}]; R_d denotes daily diffuse radiation at the canopy top [MJ m^{-2} day^{-1}]; θ denotes solar zenith angle [radian]; L denotes leaf area index [m^2 (leaf hemi-surface area) m^{-2} (ground area)]; Ω denotes foliage clumping index [dimensionless]; A_n denotes the leaf net photosynthetic rate [μmol CO_2 m^{-2} s^{-1}]; T_l denotes daily mean leaf temperature [°C]; T_a denotes daily mean air temperature [°C]; *VPD* denotes daily vapor pressure deficit [Pa]; P_{atm} denotes daily atmospheric pressure [Pa]; *Photo* denotes daily photoperiod for a given day of year at a given geolocation [hour]; *SWC* denotes the root zone soil water content [kg m^{-2}]; g_s denotes the leaf stomatal conductance [m s^{-1}]; g_b denotes the leaf boundary layer conductance [m s^{-1}]; c_i denotes the intercellular CO_2 partial pressure [Pa]; $[CO_2]$ denotes atmospheric CO2 concentration [ppm]; u denotes the wind speed [m s^{-1}]; λE_l denotes the latent heat at the leaf surface [W m^{-2}]; and λE_s denotes the evaporation rate for the soil surface [W m^{-2}].

model has proven suitable for applications in deciduous broadleaf forests when validated against direct measurements of canopy photosynthesis and evapotranspiration at flux tower sites (Xin, 2016).

The GPD model consists of several sub-models and each sub-model involves a complex system of equations. Here we only provide a brief summary for each sub-model (Table 1), where complete descriptions of the GPD model can be found in Xin (2016). The GPD model accounts for five fundamental processes within a canopy: 1) a radiative transfer model that determines the canopy light environment and the leaf radiation absorption, 2) a leaf photosynthesis model that simulates the photosynthetic rates of individual leaves, 3) a leaf conductance model that derives the leaf boundary layer and stomatal conductance, 4) a leaf energy balance model that accounts for leaf temperature and leaf transpiration, and 5) a surface energy balance model that derives soil evaporation rates. Note that the models of leaf photosynthesis, leaf transpiration, and leaf conductance are also convolved in terms of model inputs. Similar to the method used for the steady-state approximation, the canopy model can be solved iteratively until converging.

2.3. Comparative modeling based on Growing Season Index

To make comparisons with the proposed method, another method based on the Growing Season Index (GSI) is also applied for simulating LAI time series (Jolly et al., 2005; Savoy and Mackay, 2015). GSI is a simple indicator of environmental constraints to canopy development and has proven useful for monitoring canopy greenness in time series. GSI is derived as a single metric based on the product of three individual environmental indicators on a daily basis as follows:

$$iGSI = iTMIN \times iVPD \times iPhoto \tag{6}$$

where *iGSI* denotes daily growing season index, and *iTMIN*, *iVPD*, and *iPhoto* denote the daily indicator for minimum temperature, vapor pressure deficit, and photoperiod, respectively.

The indices of minimum temperature (*iTMIN*), vapor pressure deficit (*iVPD*), and photoperiod (*iPhoto*) are bounded between 0 and 1 and are derived as follows:

$$iTMIN = \max\left(0, \min\left(\frac{TMIN - TMIN_{min}}{TMIN_{max} - TMIN_{min}}, 1\right)\right) \tag{7}$$

$$iVPD = \max\left(0, \min\left(1 - \frac{VPD - VPD_{min}}{VPD_{max} - VPD_{min}}, 1\right)\right) \tag{8}$$

$$iPhoto = \max\left(0, \min\left(\frac{Photo - Photo_{min}}{Photo_{max} - Photo_{min}}, 1\right)\right) \tag{9}$$

where *TMIN* denotes daily minimum temperature [°C], *VPD* denotes daily vapor pressure deficit [Pa], *Photo* denotes daily photoperiod [hour], whereas the minimum and maximum thresholds for daily minimum temperature, daily vapor pressure deficit, and daily photoperiod that constrain vegetation growth are given as $TMIN_{\min} = -2$ °C, $TMIN_{\max} = 5$ °C, $VPD_{\min} = 900$ Pa, $VPD_{\max} = 4100$ Pa, $Photo_{\min} = 10$ h, and $Photo_{\max} = 11$ h, respectively.

The daily GSI is calculated as the 21-day simple moving average of the daily indicator (*iGSI*). Note that both GSI and *iGSI* are dimensionless, and thus both are scaled using LAI at canopy closure (LAI_c) when modeling LAI time series. An example is given in Fig. 1b to illustrate the LAI time series modeled based on GSI.

2.4. Study materials

We use measurements at flux tower sites for model development and apply our model to simulate seasonal LAI of deciduous broadleaf forest for the entire eastern United States (Fig. 2). The climate data on a daily basis are required as model inputs, whereas both LAI and GPP data are needed for model validation.

For the site-scale modeling studies, 106 site-year data from twelve flux towers of deciduous broadleaf forests (Table 2) that have Level 2 or Level 4 data available in the AmeriFlux website (http://ameriflux.ornl.gov/) were used for model validation. We used half-hourly gap-filled Level 4 data as priority and half-hourly or hourly Level 2 data as the secondary choice if Level 4 data were missing. Half-hourly or hourly flux tower measurements, such as air temperature, incoming solar radiation, atmospheric pressure, vapor pressure deficit, gross primary production, and latent heat, were preprocessed to a daily basis. Extraterrestrial solar radiation, photoperiod, and solar zenith angle (i.e., the angle that the sun away from directly overhead) are calculated as a function of geolocation (i.e., latitude and longitude), the day of year (DOY), and solar time of the day (Allen et al., 1998). Diffuse solar radiation, if not measured, was derived based on incoming solar radiation and extraterrestrial solar radiation using an empirical model recently developed for the United States (Kathilankal et al., 2014). Atmospheric pressure, if missing, is derived as a function of elevation. All functions that derive the needed but missing model inputs could be found in

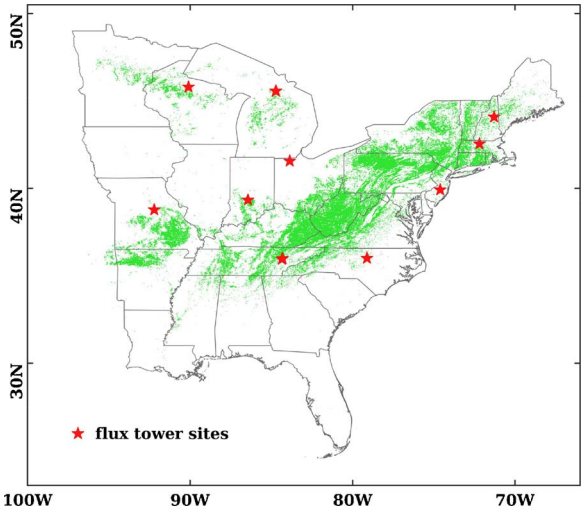

Fig. 2. Locations of the studied flux tower sites against a backdrop of the MODIS land cover classification map of deciduous broadleaf forests. Note that US-WBW is located close to US-ChR and US-UMd is located close to US-UMB.

Table 2
Site information for the flux towers of deciduous broadleaf forests.

Site Code	Site Name	Lat (°N)	Lon (°W)	Elev (m)	Years	Reference
US-Bar	Bartlett Experimental Forest	44.0646	−71.2881	272	2004–2011	Jenkins et al. (2007)
US-ChR	Chestnut Ridge	35.9311	−84.3324	286	2006–2010	Hollinger et al. (2010)
US-Dk2	Duke Forest Hardwoods	35.9736	−79.1004	168	2007–2008	Oishi et al. (2008)
US-Ha1	Harvard Forest EMS Tower	42.5378	−72.1715	340	2000–2012	Urbanski et al. (2007)
US-MMS	Morgan Monroe State Forest	39.3231	−86.4131	275	2000–2014	Dragoni et al. (2011)
US-MOz	Missouri Ozark	38.7441	−92.2000	219	2005–2013	Gu et al. (2006)
US-Oho	Oak Openings	41.5545	−83.8438	230	2005–2011	Xie et al. (2014)
US-Slt	Silas Little Experimental Forest	39.9138	−74.5960	30	2005–2012	Clark et al. (2012)
US-UMB	Univ. of Mich. Biological Station	45.5598	−84.7138	234	2000–2012	Gough et al. (2013)
US-UMd	UMBS Disturbance	45.5625	−84.6975	239	2008–2012	Gough et al. (2013)
US-WBW	Walker Branch	35.9588	−84.2874	343	2000–2006	Miller et al. (2007)
US-WCr	Willow Creek	45.8060	−90.0798	515	2000–2013	Desai et al. (2008)

details in Xin (2016).

To evaluate LAI modeling, we obtained all field-measured LAI at the flux towers from the AmeriFlux biological datasets. Because field experiments only provide insufficient LAI measurements at arbitrary time intervals, we also processed satellite data from Moderate Resolution Imaging Spectroradiometer (MODIS) that provide continuous large-scale observations of the land surface. The 8-day 500 m MODIS LAI Version 6 products (MOD15A2H; Myneni et al., 2002) and the yearly 500 m MODIS Land Cover type Version 5 products (MCD12Q1; Friedl et al., 2010) were downloaded from the Land Processes Distributed Active Archive Center (https://lpdaac.usgs.gov/). The satellite-derived LAI could fluctuate unrealistically in the time series due to cloud and/or aerosol contamination (Running and Zhao, 2015). To produce reasonable LAI time series, we first replaced poor quality LAI data as derived based on the Quality Control data in MOD15A2H using the median value of a three-point moving window and then filled the gap, if any, using the autoregressive modeling approach. Spikes in the gap-filled time series due to possible outliers are removed using the Hampel filter and then a Savitzky-Golay filter is applied to produce smoothed time series of canopy LAI on an 8-day basis, which are further linearly interpolated to daily time series (Li et al., 2014). The satellite-based LAI time series are extracted for the pixel that contains the corresponding flux tower site.

In addition to the field datasets of absolute LAI, the datasets of relative LAI developments as derived from radiometric field measurements at four deciduous broadleaf forests within our study domain (US-Ha1, US-MMS, US-UMB, and US-WCr; data from the North American Carbon Program phenology site synthesis by Richardson et al. (2012), see also Barr et al. (2013)) were used for study. Daily canopy gap fraction was first calculated as the ratio of measured daily incident solar photosynthetic photon flux density below the canopy to that above the canopy. The seasonal trajectory of canopy LAI was estimated based on canopy gap fraction and was further normalized into a relative scale to obtain relative LAI developments (0 = bare canopy in winter; 1 = full canopy in summer). The correlation between LAI derived using canopy radiation absorption and LAI measured with the LAI-2000 instruments were reported to be high ($r > 0.95$ for US-MMS and US-UMB and $r = 0.85$ for US-Ha1). More details about the processing of field data could be found in (Richardson et al., 2012).

For the large-scale modeling studies, we obtain daily 1000 m climate data for the year of 2006 from the Daymet datasets (Thornton et al., 2012) distributed by the Oak Ridge National Laboratory (ORNL) Distributed Active Archive Center (http://daymet.ornl.gov/). The climate datasets are reprojected to match the Sinusoidal projection of the MODIS data using the tool of Geospatial Data Abstraction Library. Daily mean temperature was calculated as the average of daily maximum and minimum temperatures. Daily vapor pressure deficit were derived as the difference between average saturated vapor pressure and vapor pressure. The 1000 m digital elevation maps as obtained from NOAA's Global Land One-km Base Elevation (GLOBE) project (http://www.ngdc.noaa.gov/mgg/topo/) was used to derive atmospheric pressure. Other climate data required by the model are calculated the same way as the processing of the flux tower datasets. To evaluate the model performance over large areas, the processed 500 m MODIS LAI time series were resampled to match the 1000 m climate datasets based on the averaging method for the pixels that are classified as deciduous broadleaf forests in the MODIS land cover product. The MODIS land cover product is resampled to 1000 m resolution based on the majority approach and is then used to mask out areas that are not deciduous broadleaf forests.

2.5. Model implementation

Modeling seasonal LAI time series requires proper parameterization for each individual sub-model. The GPD model that simulates canopy photosynthesis given LAI has already been well calibrated for the biome of deciduous broadleaf forests. Typical parameter values in the literature are used with details explained in Xin (2016). The leaf photosynthesis, conductance, and transpiration models were solved iteratively by initializing the leaf photosynthesis model using an intercellular to ambient carbon dioxide concentration ratio of 0.66 (Katul et al., 2000). It typically takes less than four iterations to obtain converged solutions when simulating canopy photosynthesis on a daily basis.

Given LAI time series derived from MODIS for all the flux tower sites, LAI at canopy closure (LAI_c) for deciduous broadleaf forests is determined as 5.793 based on the maximum 95th percentile of satellite-derived LAI, whereas GPP_c is determined as the mean value of daily GPP from all flux tower data for the time period that MODIS LAI are greater than LAI_c. Similar to the method used to solve canopy photosynthesis, the simultaneous equations of Eqs. (3) and (4) are solved iteratively given an initialized LAI value of 3.0, and it normally takes less than five iterations to obtain a converged solution for LAI at the steady state condition (LAI_s). The same as the GSI model, the sample window size (n) for simple moving average to account for the time lagging effect is set as 21, thereby allowing for direct comparisons.

As the correlation between modeled and observed seasonal trajectory of canopy LAI could be high because of the underlying seasonality, key phenophases from the seasonal trajectory of both modeled and observed canopy LAI were also extracted for model assessment. The phenological transition dates we estimated were derived for the first spring and last autumn dates at which measured and modeled LAI = 20%, 50%, and 80% of the seasonal LAI amplitude (Richardson et al., 2012). The relative thresholds (20%, 50%, and 80%) were chosen to represent varied key phenophases in vegetation growth. The phenological transition dates derived from modeled canopy LAI were then compared with those derived from observed canopy LAI.

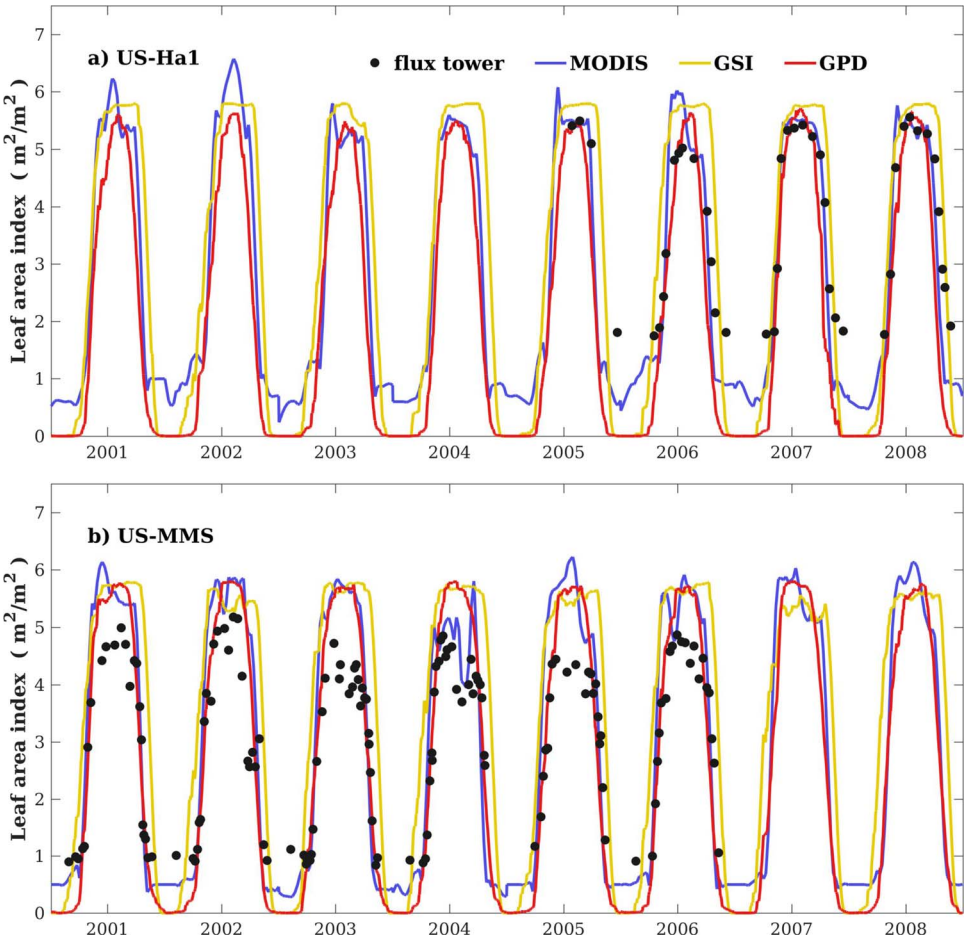

Fig. 3. Measured and modeled daily time series of leaf area index are shown for the flux tower sites of a) US-Ha1 and b) US-MMS over 8 successive years from 2001 to 2008.

3. Results

3.1. Site-scale modeling of leaf area index and leaf phenology

The measured and modeled time series of LAI are shown for 8 successive years over the US-Ha1 and US-MMS sites in Fig. 3. Overall, the LAI modeled using both GPD and GSI match with LAI measured in field experiments or derived from MODIS in terms of the phase and amplitude. Seasonal LAI peaks derived from MODIS agree with that measured in field experiments for the US-Ha1 site, but are slight overestimated for the US-MMS site. As the prescribed parameter of LAI at canopy closure was calibrated using MODIS data, the modeled seasonal LAI amplitudes match with satellite-based time series better than field-based time series. For the deciduous broadleaf forests, modeled LAI could be as low as zero during the wintertime, given that the climate conditions are not suitable for vegetation growth, while MODIS-derived LAI could have residual values. GPD-based LAI exhibits time series of seasonal cycles closer to MODIS-based LAI than GSI-based LAI in phase, as GSI-based LAI tends to overestimate during the period from spring onset to summer maturation and from autumn senescence to winter dormancy.

Scatter plots in Fig. 4 show the validation of modeled and satellite-based LAI against field-measured LAI. Despite having mismatched footprints, satellite data provide reasonable LAI estimates as compared to field measurements, where the coefficient of determination (R^2) is as high as 0.803 and the root mean square error (RMSE) is 0.972 m^2/m^2. The LAI modeled using GPD agree well with field measurements (R^2 = 0.801 and RMSE = 0.924 m^2/m^2). By comparisons, the LAI modeled using GSI, although correlating with field-measured LAI positively and significantly, have relatively large errors (RMSE = 1.696 m^2/m^2). When validating using field measured LAI, positive biases (the metric of bias, derived as the mean of the residual errors between modeled and observed data, is indicative to whether the model tends to under- or over-estimate the measured data with an ideal value of zero; Bennett et al. (2013)) are apparent for MODIS-based LAI (bias = 0.326 m^2/m^2) and GSI-based LAI (bias = 1.409 m^2/m^2), and biases are minor for GPD-based LAI (bias = −0.070 m^2/m^2). The GSI-based LAI have shown to slightly underestimate during the non-growing season but largely overestimate during the growing season.

Relative LAI developments (0 = bare canopy in winter; 1 = full canopy in summer) are evaluated against that derived from continuous measurements of Fraction of absorbed Photosynthetically Active Radiation (FPAR) at four sites of deciduous broadleaf forests on a weekly basis (Fig. 5). The correlation coefficients (r) between relative LAI from the GPD model and field measurements are significantly high (r = 0.92, 0.97, 0.95, and 0.98 for US-Ha1, US-MMS, US-UMB, and US-WCr, respectively). The correlation coefficients between relative LAI from the GSI model and field measurements are slightly lower (r = 0.93, 0.89, 0.89, and 0.90 for US-Ha1, US-MMS, US-UMB, and US-WCr, respectively) for all sites except US-Ha1. Note that relative LAI as derived from the GSI model are positively biased (bias = 0.12, 0.15, 0.15, and 0.12 for US-Ha1, US-MMS, US-UMB, and US-WCr, respectively), whereas relative LAI as derived from the GPD model do not have significant biases.

In addition to evaluation using field measurements, the modeled results are assessed using the processed MODIS LAI on a biweekly basis for all flux towers in Fig. 6. The GPD model and the GSI model could explain 92.9% and 73.1% variance of the MODIS LAI, respectively. The GPD-based LAI and MODIS LAI have a regression line close to the line of equality and an RMSE value of 0.650 m^2/m^2. Note that the GPD-based

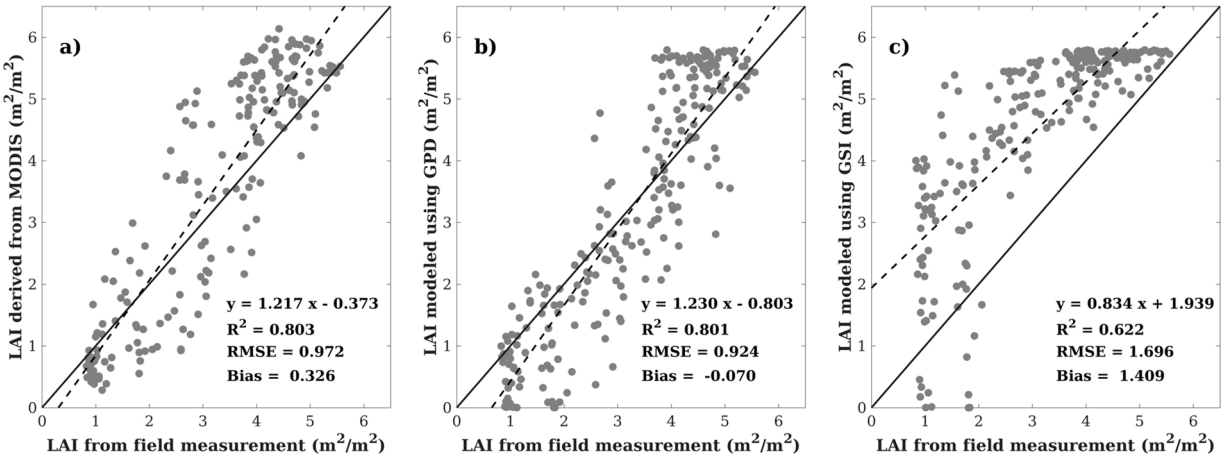

Fig. 4. Regressions are shown for comparisons a) between field-measured and satellite-based LAI, b) between field-measured and GPD-based LAI, and c) between field-measured and GSI-based LAI using all available data from the deciduous broadleaf forest sites. The solid lines denote the lines of equality and the dashed lines denote the regression lines.

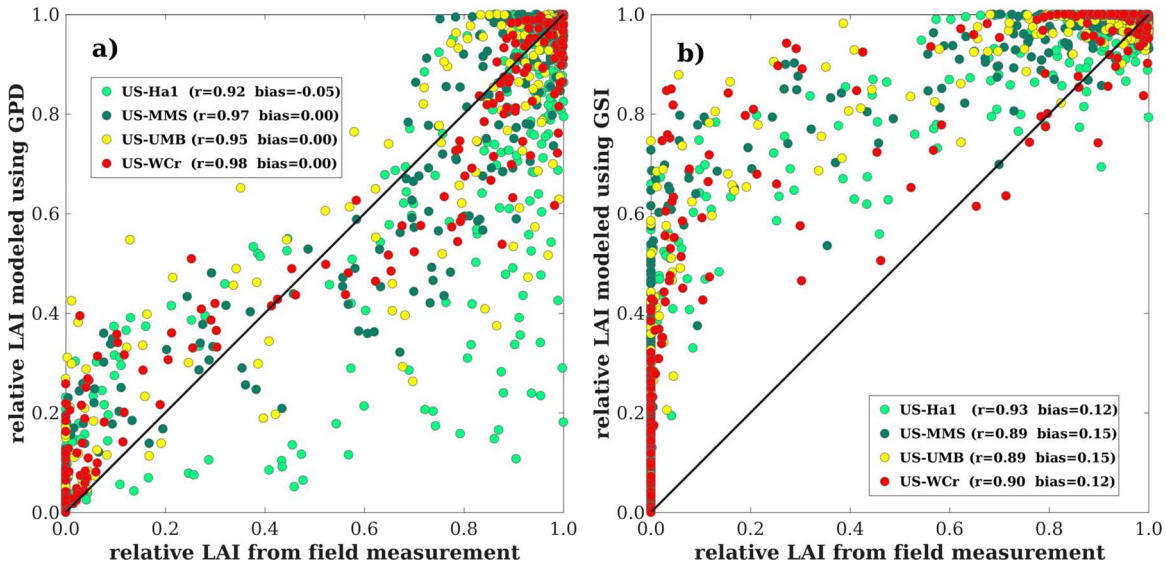

Fig. 5. Regressions are shown for comparisons a) between field-measured and GPD-based relatively LAI and b) between field-measured and GSI-based relatively LAI on a weekly basis. All available site-year flux tower data were included in the analysis. The solid lines denote the lines of equality.

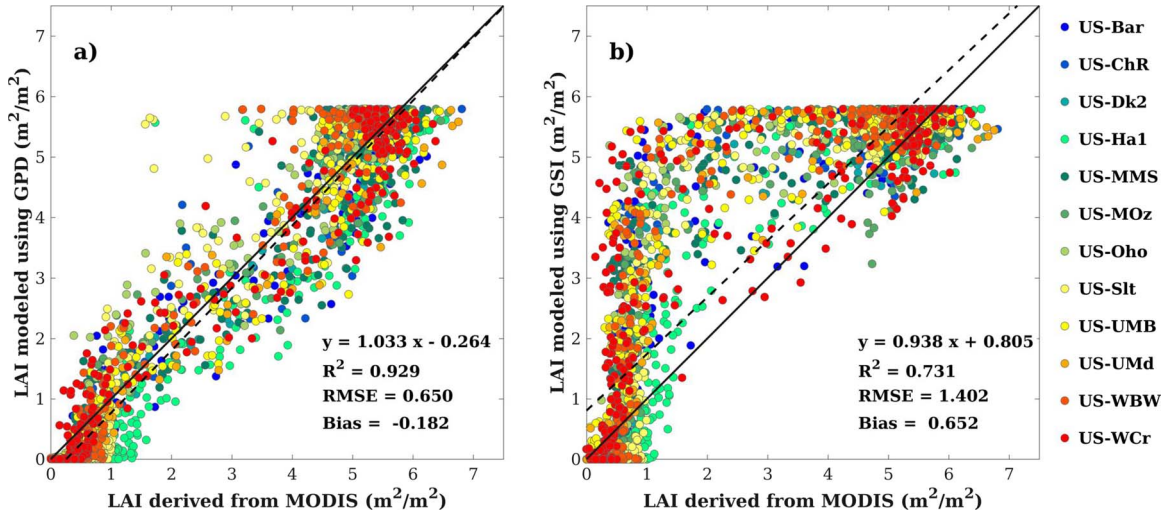

Fig. 6. Regressions are shown for comparisons a) between MODIS-based and GPD-based LAI and b) between MODIS-based and GSI-based LAI on a biweekly basis. All available site-year flux tower data were included in the analysis. The solid lines denote the lines of equality and the dashed lines denote the regression lines.

Table 3
The performance of predicted leaf area index (LAI) transition dates as evaluated against field measurements and satellite observations. LAI transition dates were estimated based on dates at which specific relative thresholds of seasonal development, i.e., 20%, 50%, 80% of seasonal amplitude, were reached. Positive biases indicate that modeled spring onset and/or autumn senescence are later than observed ones, and negative biases indicate the opposite.

reference	GPD-based method			GSI-based method		
	RMSE (days)	Bias (days)	r	RMSE (days)	Bias (days)	r
field data (n = 27 site-years)						
Spring LAI 20% threshold	0.916***	12.97	−12.19	0.761***	38.12	−36.89
Spring LAI 50% threshold	0.924***	4.60	−1.11	0.805***	21.92	−19.82
Spring LAI 80% threshold	0.710***	12.07	6.41	0.618***	16.12	−10.82
Autumn LAI 80% threshold	−0.086	26.61	−17.59	0.020	28.80	21.26
Autumn LAI 50% threshold	0.456*	17.71	−14.67	0.683***	20.98	19.26
Autumn LAI 20% threshold	0.480*	9.92	−2.33	0.690***	28.44	27.22
MODIS data (n = 104 site-years)						
Spring LAI 20% threshold	0.835***	10.89	−7.88	0.793***	35.57	−33.64
Spring LAI 50% threshold	0.752***	9.92	0.27	0.737***	27.97	−24.39
Spring LAI 80% threshold	0.612***	14.79	7.77	0.586***	21.30	−13.30
Autumn LAI 80% threshold	−0.043	15.04	0.12	−0.058	42.65	39.82
Autumn LAI 50% threshold	0.619***	7.60	0.27	0.536***	34.84	33.91
Autumn LAI 20% threshold	0.707***	9.78	6.72	0.636***	34.97	34.23

* Correlation is significant at the 0.05 level.
*** Correlation is significant at the 0.001 level.

LAI have a negative bias as compared to MODIS LAI, which offset the positive bias of MODIS LAI as compared to the field-measured LAI. By comparison, the GSI-based LAI have an RMSE value of 1.402 m^2/m^2 and a positive bias value of 0.652 m^2/m^2 when taking MODIS LAI as references. As validated using the site-scale data, the GPD model shows to be robust for simulating seasonal dynamics of canopy LAI.

Table 3 provides assessments of the timing of seasonal phenology transitions as derived from both the GPD and GSI models using both field measurements and satellite observations. Using field data from four sites, the GPD model could well simulate the first date at which daily spring LAI exceeds 50% seasonal amplitude with the correlation coefficient of 0.924 and the bias of −1.11 days. By comparison, the GSI-based method predicts the timing of key phenophases in spring much earlier than field measurements (bias = −36.89, −19.82, and −10.82 days for spring LAI that exceeds 20%, 50%, 80% seasonal amplitudes, respectively). In autumn, the GPD model predicts the last date at which LAI exceeds 20% seasonal amplitude close to field observations (r = 0.480 and bias = −2.33 days), whereas the predictions based on the GSI model are much later than was actually observed (r = 0.690 and bias = 27.22 days).

Given that data from field observations were limited (n = 27 site-years), key phenophases derived from MODIS LAI were also used for model assessment (n = 104 site-years). With large site-year datasets from satellites, the GPD model could well simulate key phenophases both in spring (r = 0.835 and bias = −7.88 days for the first dates that LAI exceeds 20% seasonal amplitudes) and in autumn (r = 0.707 and bias = 6.72 days for the last dates that LAI exceeds 20% seasonal amplitudes). Similar to assessment using field observations, the GSI-based method predicts the timing of key phenophases much earlier in spring (large negative biases) and much later in autumn (large positive biases) than derived from satellite data. Note that in terms of modeling key phenophases in spring and fall, the GSI model generally performed as well as or better than 14 tested models in Richardson et al. (2012), while the GPD model greatly exceeded the performance of any single model in that earlier study.

3.2. Large-scale modeling of leaf area index

To understand the model performance over large areas, Fig. 7 presents annual average LAI as obtained using different methods for the eastern United States. The annual average LAI in the year of 2006 simulated using the GPD model (Fig. 7b) has a spatial pattern similar to that derived from satellite data (Fig. 7a), where both show to increase from less than 2.0 m^2/m^2 in the north to greater than 3.0 m^2/m^2 in the south. Notably, the GPD-based method could well depict the decreases of LAI as elevation increases in the Appalachian mountain areas. Compared to the MODIS data, the GSI-based method (Fig. 7c), although producing a minor north-south gradient of LAI, largely overestimates LAI, given that the annual average LAI are greater than 3.0 m^2/m^2 for most areas.

Fig. 8 displays the spatial pattern of the Pearson's correlation coefficient between modeled and satellite-based daily LAI time series in 2006, where higher positive correlations indicate better modeling of LAI for the corresponding pixel. The GPD model well captures the seasonal variation of satellite-derived LAI, as the correlation coefficients are higher than 0.95 across the eastern United States. By comparison, although the GSI-based LAI time series have a positive correlation with that derived from MODIS, the correlation coefficients only

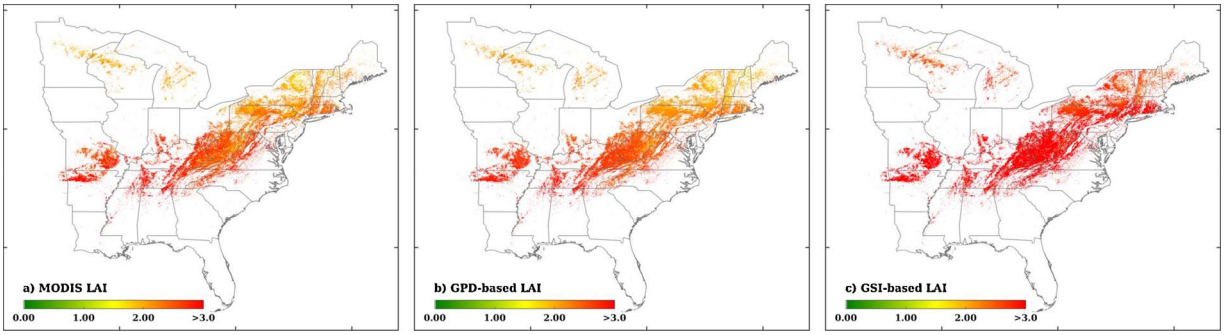

Fig. 7. The spatial distribution of annual average leaf area index as derived from a) MODIS, b) the GPD model, and c) the GSI model for the year of 2006 across the eastern United States.

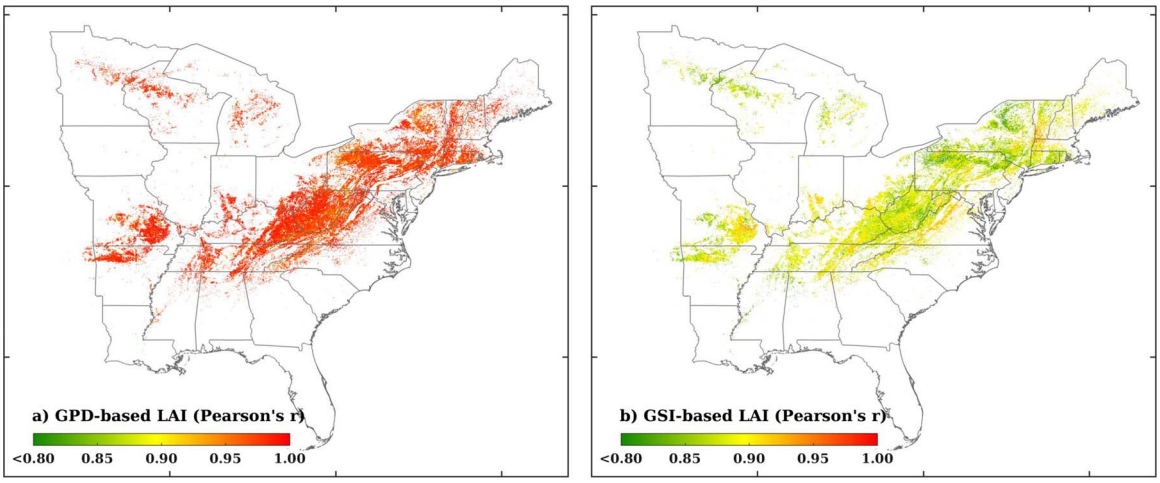

Fig. 8. The spatial distribution of Pearson's correlation coefficients a) between GPD-modeled LAI and satellite-derived LAI and b) between GSI-modeled LAI and satellite-derived LAI for the year of 2006 across the eastern United States. The Pearson's r values that are greater than 0.80 are all significant at the 0.001 level.

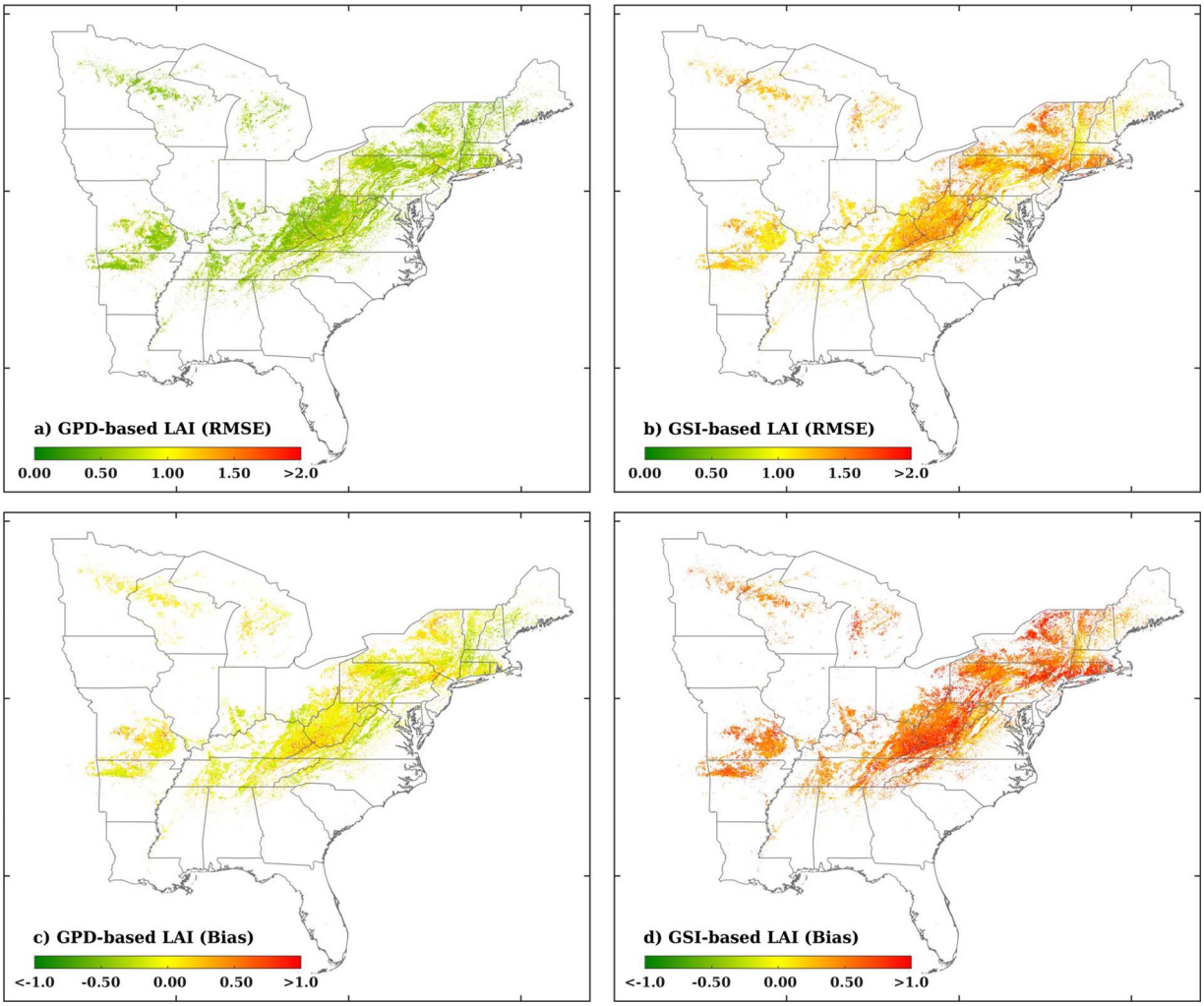

Fig. 9. The spatial distribution of errors are shown for a) RMSE between GPD-modeled LAI and satellite-derived LAI, b) RMSE between GSI-modeled LAI and satellite-derived LAI, c) bias errors between GPD-modeled LAI and satellite-derived LAI, and d) bias errors between GSI-modeled LAI and satellite-derived LAI for the year of 2006 across the eastern United States.

range from 0.80 to 0.90 for most areas, much lower than that between GPD-based and satellite-based LAI.

To help further understand the model performance over large areas, Fig. 9 presents the spatial distribution of the errors between modeled and satellite-based LAI time series in the year of 2006. The RMSE between the GPD-modeled and satellite-derived LAI are about 0.5 m^2/m^2 for most of the study areas, much lower than that between GSI-modeled and satellite-derived LAI, which vary from 1.0 to over 2.0 m^2/m^2 across the eastern United States. The bias errors between the GPD-modeled and MODIS-based LAI mostly range from -0.5 to 0.5 m^2/m^2,

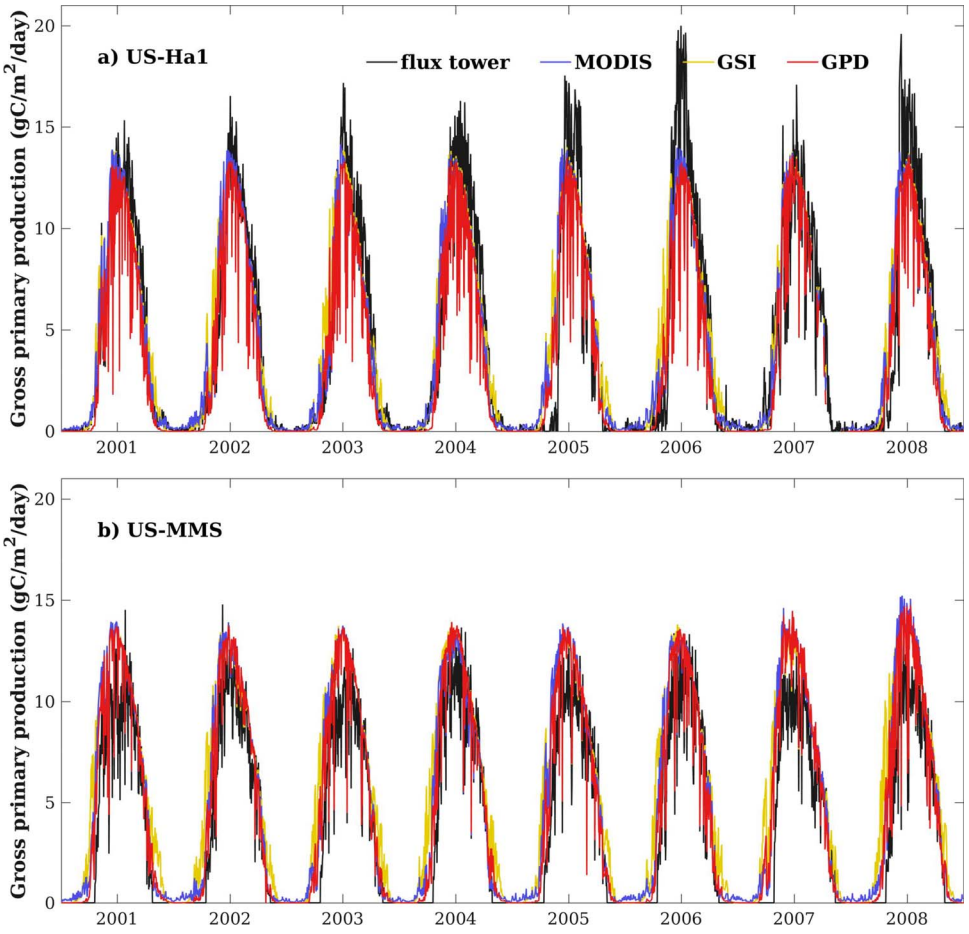

Fig. 10. Measured and modeled daily time series of gross primary production are shown for the flux tower sites of a) US-Ha1 and b) US-MMS over 8 successive years from 2001 to 2008. All the modeled gross primary production is derived by substituting satellite-based and modeled LAI into the GPD model separately.

while the GSI-based method results in positive LAI bias errors as shown to be greater than 0.5 or even 1.0 for most areas. The magnitudes of errors in terms of RMSE and biases obtained at a large scale are consistent with those derived at the site scale. Note that the spatial distribution of errors does not exhibit any apparent geographical gradient for the GPD-modeled results, while there are large RMSE and bias errors in the Appalachian mountain areas and at high latitudes for the GSI-modeled results, implying that the GSI model is more susceptible to bias in cooler climates.

3.3. Site-scale modeling of gross primary production

An important issue in modeling seasonal leaf dynamics is whether the modeled LAI can be used for subsequent modeling of canopy photosynthesis. To address the question, all modeled and satellite-derived LAI time series are substituted into the GPD model to simulate daily canopy GPP, of which the time series are compared with flux tower measurements in Fig. 10. Compared with flux tower measurements, the modeled GPP time series are lower for the US-Ha1 site and slightly higher for the US-MMS site over the 8 successive years in general, of which the differences are likely due to different canopy structures across both sites of deciduous broadleaf forests. The modeled GPP could well capture daily variation in time series resulted by reduced incoming solar radiation due to clouds. Interestingly, the GPP time series modeled using GSI-based LAI agree with others, although the GSI-based LAI are much higher than others during the time period of spring onset and autumn senescence. One reason is that the climate condition poses large limitations on canopy photosynthetic activities when the canopy is not closed even if the modeled LAI are unrealistically high.

When validating against GPP measured at flux towers on a biweekly basis, canopy GPP modeled using MODIS-derived LAI, GPD-based LAI, and GSI-based LAI result in R^2 values of 0.851, 0.848, and 0.799, respectively, RMSE values of 1.962, 1.932, and 2.400 gC/m^2/day, respectively, and bias values of 0.629, 0.476, and 1.054 gC/m^2/day, respectively (Fig. 11). As satellite-derived LAI are likely overestimated during the non-growing season, the GPD-based method provides lower biased estimates of GPP than using the satellite-based data. The GSI-based method produces the largest GPP overestimates as compared to flux tower measurements. Since GPP modeled using both satellite-derived and GPD-based LAI agree reasonably well with flux tower GPP and achieve comparable performance, the GPD-based method shows to provide a robust basis for modeling leaf dynamics as well as canopy photosynthesis.

4. Discussion

4.1. Relationship between the GPD- and GSI-based method

As both GPD- and GSI-based models adopt the method of simple moving average to simulate time series of canopy LAI, there is a need to explore and understand the relationship between the two models. We therefore vary the parameters in Eq. (3) (i.e., let $LAI_c/GPP_c = 1$) while holding other parameters unchanging, and apply the GPD model to simulate LAI time series again. Fig. 12a presents an example for the LAI time series derived from different approaches for the site of US-Oho in 2011. While the proposed GPD-based method agrees with satellite-derived LAI, the recalibrated GPD-based model produces LAI time series that are consistent with the GSI-based method. When making direct

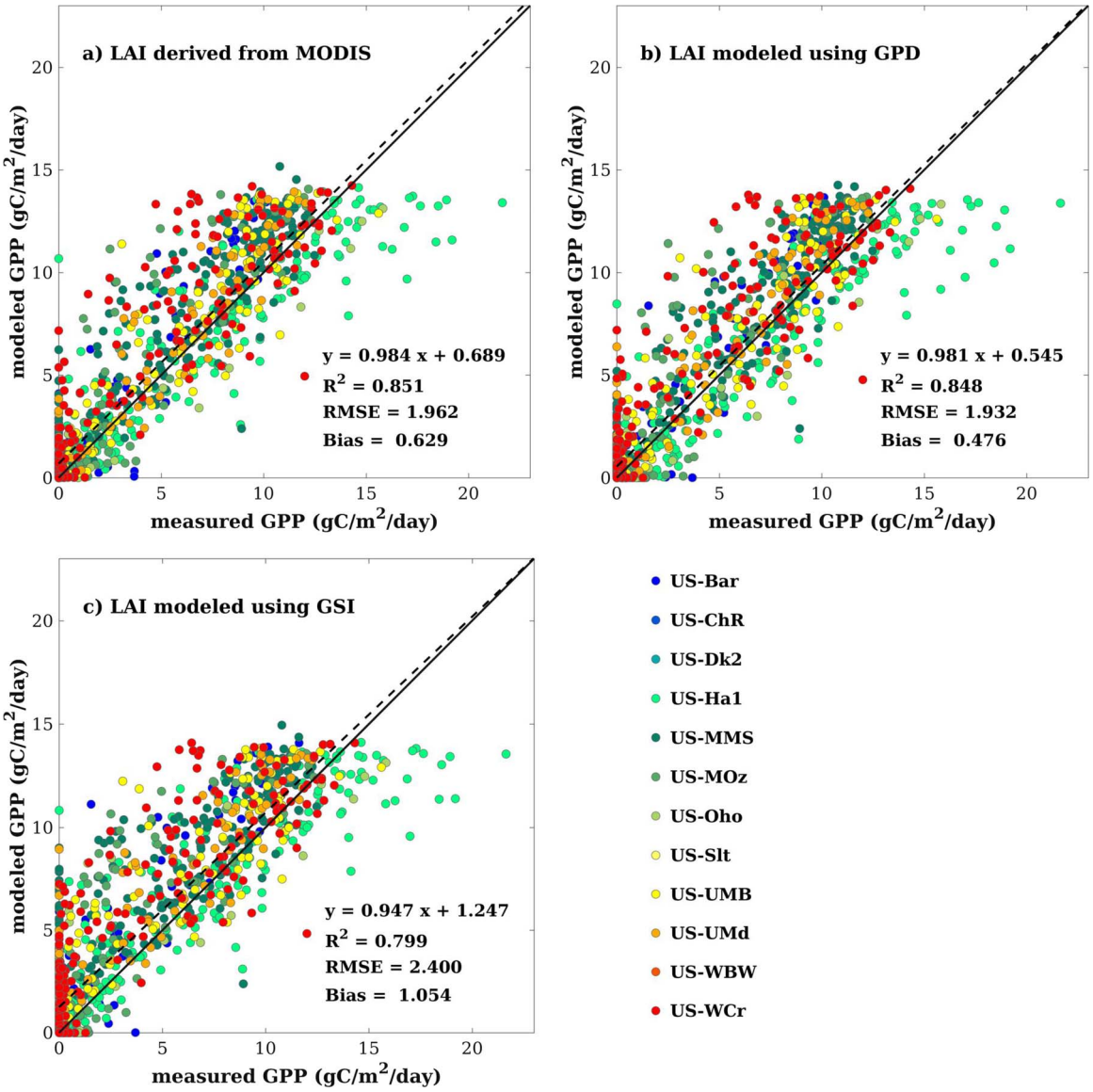

Fig. 11. Regressions are shown for comparisons a) between GPP measured at flux towers and GPP modeled using MODIS-derived LAI, b) between GPP measured at flux towers and GPP modeled using GPD-derived LAI, and c) between GPP measured at flux towers and GPP modeled using GSI-derived LAI on a biweekly basis. All available site-year flux tower data were included in the analysis. The solid lines denote the lines of equality and the dashed lines denote the regression lines.

comparisons between modeled LAI using all biweekly flux tower data as shown in Fig. 12c, the GSI-based method has large positive biases over the proposed GPD-based method (Fig. 12b), but matched results with that obtained from the recalibrated GPD-based method (R^2 = 0.952, RMSE = 0.540 m^2/m^2, and bias = 0.042 m^2/m^2). These results suggest that the GPD-based method, if recalibrated, could produce nearly the same results as compared to the GSI-based method.

In essence, the proposed GPD-based model is a highly generalized method that includes considerations for all environmental factors influencing vegetation growth, and the GSI-based model is a much simplified method that only accounts for the impacts of dominate climate drivers (i.e., daily minimum temperature, vapor pressure deficit, and photoperiod) on vegetation photosynthetic activities. Note that GSI has a mathematical form analogous to the Jarvis-Stewart equation (Bonan, 2002; Jarvis and McNaughton, 1986), which has been widely used for modeling stomatal conductance and also vegetation productivity, but cancels out the term of LAI in Eq. (3) to generate a simplified and dimensionless bioclimatic index. Both the GPD- and GSI-based methods first seek leading metrics that are indicative of the climate suitability to vegetation growth and then account for the time lagging effects, thereby simulating the dynamics of vegetation leaf allocation.

4.2. Future improvements and applications

While the GPD-based method shows to simulate seasonal variation of leaf dynamics in deciduous broadleaf forests successfully using climate variables, one important issue is whether the developed method could capture the interannual variation of plant leaf dynamics. Recently, we have developed the GPD model that is able to well simulate multi-decadal variation in the timing of vegetation spring onset across the Northern Hemisphere (Xin, 2016). Since the method developed here is one step forward in addition to our previous study and provides a complete rather than an empirical solution, applying the GPD-based method using long-term time series data has the potential for simulating interannual variation of plant leaf dynamics. Evaluating the model against extensive long-term data sets is beyond the scope of the current research, but is urgently needed to fully validate our approach.

Another key issue is to understand whether the developed method can be applied over other biomes and other places. Although GSI has

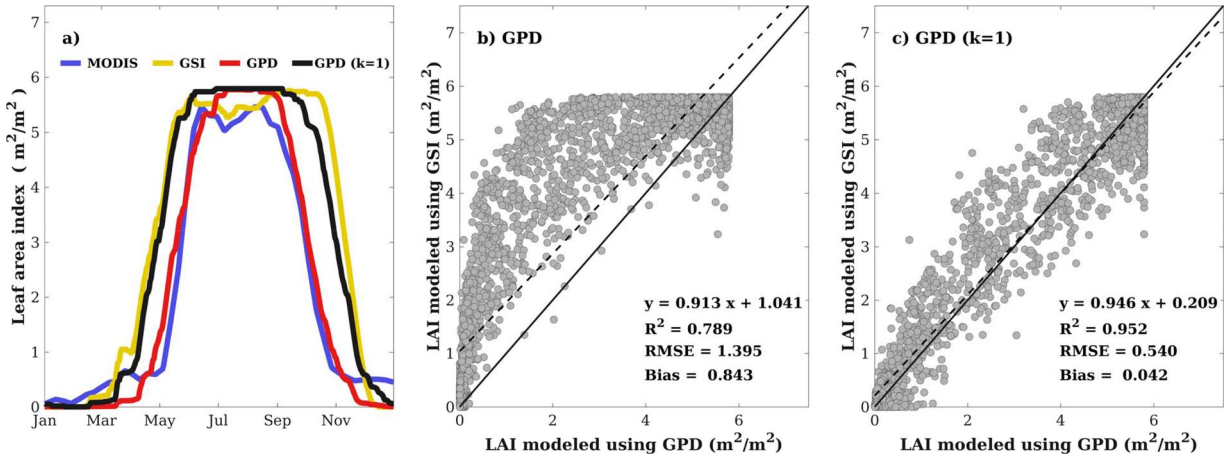

Fig. 12. The relationship between GPD and GSI models are illustrated for a) time series of satellite-derived and modeled leaf area index, b) comparisons between GSI-based LAI and the proposed GPD-based LAI on a biweekly basis, and c) comparisons between GSI-based LAI and the recalibrated GPD-based LAI on a biweekly basis. The recalibrated GPD method applies $k = 1$ m^2 day/gC in modeling, where $k = LAI_c/GPP_c$ denotes leaf area index per gross primary production at canopy closure. In Fig. 12b and 12c, the solid lines denote the lines of equality and the dashed lines denote the regression lines. Data are shown for the entire year of 2011 at the US-Oho site in Fig. 12a and all available site-year flux tower measurements in Fig. 12b and 12c.

been developed as a generalized index to simulate time series of vegetation greenness across biomes, GSI only accounts for water availability indirectly using vapor pressure deficit, while soil moisture and precipitation have large impacts on the phenology of short vegetation like grasses, whose roots are not long enough to fetch deep water. Having a similar mathematical form as compared to GSI, the GPD-based method accounts for a wider range of environmental factors influencing vegetation growth and therefore could potentially improve the simulation of leaf allocation dynamics for plants in arid ecosystems, where existing phenology models are known to perform poorly.

It is worth noting that the performance of the proposed method is largely dependent on how accurate the canopy photosynthesis can be modeled. As shown in Fig. 11, the current version of the GPD model, which accounts for major processes within canopies, performs well when simulating canopy photosynthesis of deciduous broadleaf forests for all flux tower sites using both satellite-derived and modeled LAI. Given that a variety of land surface models have been developed to simulate plant activities with varied degrees of sophistication, it is then interesting to implement the developed approach to existing land surface models and make comparative studies of vegetation phenology for further assessments. However, advanced parameterization of land surface processes with increased sophistication in model structures often requires matching observational data, which are sometimes not available for large-scale applications.

5. Conclusions

Vegetation growing cycle, as characterized by seasonal variation of leaf dynamics, controls plant photosynthetic activities and subsequent physical and biochemical processes within canopies. As vegetation growing is highly sensitive to climate variation, one central task in land surface modeling is to develop phenology models that are capable of capturing seasonal and interannual variation of vegetation leaf allocations using environmental variables.

In this paper, we develop a new method to model seasonal variation of leaf area index (LAI) based on the idea that plant photosynthetic productivity can serve as a synthesized metric to track the climate suitability to plant growth over time. The proposed method combines the Growing Production-Day (GPD) model for simulating canopy photosynthesis and a phenology model to form closed simultaneous equations. The LAI time series is first solved iteratively to obtain the steady-state approximation without considering the time lags of plant leaf allocation in response to climate variation, and is then derived using the method of simple moving average to account for the time lagging effects. The proposed method simulates seasonal LAI well as evaluating using both field-measured and satellite-derived data, and performs better than the method based on Growing Season Index (GSI) in terms of higher correlation coefficients and lower root mean square errors. The proposed method provides a complete solution to modeling seasonal canopy leaf dynamics and gross primary production solely using climate variables.

Acknowledgments

We thank the researchers and investigators that are involved in the data collection and analysis at the AmeriFlux sites. This research is supported by National Key R&D Program of China (grant no. 2017YFA0604302 and 2017YFA0604402) and Key Projects for Young Teachers at Sun Yat-sen University (grant no. 17lgzd02). Research at the Bartlett Experimental Forest is supported by the USDA Forest Service's Northern Research Station, the National Science Foundation (DEB-1114804), and the Northeastern States Research Cooperative. ADR acknowledges additional support from the National Science Foundation's Macrosystems Biology (awards EF-1065029 and EF-1702697). We also thank anonymous reviewers for their constructive comments.

References

Allen, R.G., Pereira, L.S., Raes, D., Smith, M., 1998. Crop Evapotranspiration-Guidelines for Computing Crop Water Requirements-FAO Irrigation and Drainage Paper 56, vol. 300 FAO, Rome 6541.
Arora, V.K., Boer, G.J., 2005. A parameterization of leaf phenology for the terrestrial ecosystem component of climate models. Global Change Biol. 11 (1), 39–59.
Barr, A.G., et al., 2013. NACP Site: Tower Meteorology, Flux Observations with Uncertainty, and Ancillary Data. ORNL Distributed Active Archive Center.
Beer, C., et al., 2010. Terrestrial gross carbon dioxide uptake: global distribution and covariation with climate. Science 329 (5993), 834–838.
Bennett, N.D., et al., 2013. Characterising performance of environmental models. Environ. Modell. Softw. 40, 1–20.
Bonan, G.B., 2002. Ecological Climatology: Concepts and Applications. Cambridge University Press.
Broich, M., et al., 2014. Land surface phenological response to decadal climate variability across Australia using satellite remote sensing. Biogeosciences 11 (18), 5181–5198.
Chuine, I., Cour, P., Rousseau, D.D., 1999. Selecting models to predict the timing of flowering of temperate trees: implications for tree phenology modelling. Plant Cell Environ. 22 (1), 1–13.
Clark, D., et al., 2011. The Joint UK Land Environment Simulator (JULES), model description-part 2: carbon fluxes and vegetation dynamics. Geosci. Model Dev. 4 (3), 701.
Clark, K.L., Skowronski, N., Gallagher, M., Renninger, H., Schäfer, K., 2012. Effects of invasive insects and fire on forest energy exchange and evapotranspiration in the

New Jersey pinelands. Agric. For. Meteorol. 166, 50–61.
Dai, Y., et al., 2003. The common land model. Bull. Am. Meteorol. Soc. 84 (8), 1013–1023.
Desai, A.R., et al., 2008. Influence of vegetation and seasonal forcing on carbon dioxide fluxes across the Upper Midwest, USA: implications for regional scaling. Agric. For. Meteorol. 148 (2), 288–308.
Dragoni, D., et al., 2011. Evidence of increased net ecosystem productivity associated with a longer vegetated season in a deciduous forest in south-central Indiana, USA. Global Change Biol. 17 (2), 886–897.
Eagleson, P.S., 2005. Ecohydrology: Darwinian Expression of Vegetation Form and Function. Cambridge University Press.
Friedl, M.A., et al., 2010. MODIS Collection 5 global land cover: algorithm refinements and characterization of new datasets. Remote Sens. Environ. 114 (1), 168–182.
Friedl, M.A., et al., 2014. A tale of two springs: using recent climate anomalies to characterize the sensitivity of temperate forest phenology to climate change. Environ. Res. Lett. 9 (5), 054006.
Ganguly, S., Friedl, M.A., Tan, B., Zhang, X., Verma, M., 2010. Land surface phenology from MODIS: characterization of the Collection 5 global land cover dynamics product. Remote Sens. Environ. 114 (8), 1805–1816.
Givnish, T.J., 1986. On the Economy of Plant Form and Function: Proceedings of the Sixth Maria Moors Cabot Symposium, Evolutionary Constraints on Primary Productivity, Adaptive Patterns of Energy Capture in Plants, Harvard Forest, August 1983, vol. 6 Cambridge University Press.
Gough, C.M., et al., 2013. Sustained carbon uptake and storage following moderate disturbance in a Great Lakes forest. Ecol. Appl. 23 (5), 1202–1215.
Gu, L., et al., 2006. Direct and indirect effects of atmospheric conditions and soil moisture on surface energy partitioning revealed by a prolonged drought at a temperate forest site. J. Geophys. Res.: Atmos. 111 (D16).
Hollinger, D.Y., et al., 2010. Albedo estimates for land surface models and support for a new paradigm based on foliage nitrogen concentration. Global Change Biol. 16 (2), 696–710.
Hufkens, K., et al., 2012. Linking near-surface and satellite remote sensing measurements of deciduous broadleaf forest phenology. Remote Sens. Environ. 117, 307–321.
Jarvis, P.G., McNaughton, K., 1986. Stomatal control of transpiration: scaling up from leaf to region. Adv. Ecol. Res. 15, 1–49.
Jenkins, J., et al., 2007. Refining light-use efficiency calculations for a deciduous forest canopy using simultaneous tower-based carbon flux and radiometric measurements. Agric. For. Meteorol. 143 (1), 64–79.
Jolly, W.M., Nemani, R., Running, S.W., 2005. A generalized, bioclimatic index to predict foliar phenology in response to climate. Global Change Biol. 11 (4), 619–632.
Kathilankal, J., O'Halloran, T., Schmidt, A., Hanson, C., Law, B., 2014. Development of a Semi-parametric PAR (Photosynthetically Active Radiation) Partitioning Model for the United States, Version 1.0.
Katul, G., Ellsworth, D., Lai, C.T., 2000. Modelling assimilation and intercellular CO2 from measured conductance: a synthesis of approaches. Plant Cell Environ. 23 (12), 1313–1328.
Keenan, T.F., et al., 2013. Increase in forest water-use efficiency as atmospheric carbon dioxide concentrations rise. Nature 499 (7458), 324–327.
Li, L., et al., 2014. Mapping crop cycles in China using MODIS-EVI time series. Remote Sens. 6 (3), 2473–2493.
Li, C., 2000. Modeling trace gas emissions from agricultural ecosystems. Nutr. Cycl. Agroecosyst. 58 (1–3), 259–276.
Melaas, E.K., et al., 2013. Using FLUXNET data to improve models of springtime vegetation activity onset in forest ecosystems. Agric. For. Meteorol. 171, 46–56.
Melaas, E.K., Friedl, M.A., Richardson, A.D., 2016. Multiscale modeling of spring phenology across Deciduous Forests in the Eastern United States. Global Change Biol. 22 (2), 792–805.
Menzel, A., 2002. Phenology: its importance to the global change community. Clim. Change 54 (4), 379–385.
Miller, G.R., Baldocchi, D.D., Law, B.E., Meyers, T., 2007. An analysis of soil moisture dynamics using multi-year data from a network of micrometeorological observation sites. Adv. Water Resour. 30 (5), 1065–1081.
Myneni, R.B., et al., 2002. Global products of vegetation leaf area and fraction absorbed PAR from year one of MODIS data. Remote Sens. Environ. 83 (1–2), 214–231.
Oishi, A.C., Oren, R., Stoy, P.C., 2008. Estimating components of forest evapotranspiration: a footprint approach for scaling sap flux measurements. Agric. For. Meteorol. 148 (11), 1719–1732.
Oleson, K., et al., 2013. Technical Description of Version 4.5 of the Community Land Model (CLM). NCAR. National Center for Atmospheric Research (NCAR), Boulder, Colorado.
Richardson, A.D., et al., 2012. Terrestrial biosphere models need better representation of vegetation phenology: results from the North American Carbon Program Site Synthesis. Global Change Biol. 18 (2), 566–584.
Running, S., Zhao, M., 2015. User's Guide Daily GPP and Annual NPP (MOD17A2/A3) Products NASA Earth Observing System MODIS Land Algorithm. Version, 3. pp. 1–28.
Running, S.W., Thornton, P.E., Nemani, R., Glassy, J.M., 2000. Global terrestrial gross and net primary productivity from the earth observing system. Methods Ecosyst. Sci. 44–57.
Ryu, Y., et al., 2011. Integration of MODIS land and atmosphere products with a coupled-process model to estimate gross primary productivity and evapotranspiration from 1 km to global scales. Global Biogeochem. Cycles 25 (4), GB4017.
Savoy, P., Mackay, D.S., 2015. Modeling the seasonal dynamics of leaf area index based on environmental constraints to canopy development. Agric. For. Meteorol. 200, 46–56.
Sellers, P., et al., 1996. A revised land surface parameterization (SiB2) for atmospheric GCMs. Part I: model formulation. J. Clim. 9 (4), 676–705.
Sellers, P.J., 1985. Canopy reflectance, photosynthesis and transpiration. Int. J. Remote Sens. 6 (8), 1335–1372.
Thornton, P., et al., 2012. Daymet: Daily Surface Weather on a 1 km Grid for North America, 1980–2008. Oak Ridge National Laboratory Distributed Active Archive Center, Oak Ridge, T, N.
Urbanski, S., et al., 2007. Factors controlling CO2 exchange on timescales from hourly to decadal at Harvard Forest. J. Geophys. Res.: Biogeosci. 112 (G2).
White, M.A., Thornton, P.E., Running, S.W., 1997. A continental phenology model for monitoring vegetation responses to interannual climatic variability. Global Biogeochem. Cycles 11 (2), 217–234.
Xie, J., et al., 2014. Long-term variability and environmental control of the carbon cycle in an oak-dominated temperate forest. For. Ecol. Manage. 313, 319–328.
Xin, Q., Broich, M., Zhu, P., Gong, P., 2015a. Modeling grassland spring onset across the Western United States using climate variables and MODIS-derived phenology metrics. Remote Sens. Environ. 161, 63–77.
Xin, Q., Gong, P., Li, W., 2015b. Modeling photosynthesis of discontinuous plant canopies by linking the Geometric Optical Radiative Transfer model with biochemical processes. Biogeosciences 12 (11), 3447–3467.
Xin, Q., Gong, P., Suyker, A.E., Si, Y., 2016. Effects of the partitioning of diffuse and direct solar radiation on satellite-based modeling of crop gross primary production. Int. J. Appl. Earth Obs. Geoinf. 50, 51–63.
Xin, Q., 2016. A risk-benefit model to simulate vegetation spring onset in response to multi-decadal climate variability: theoretical basis and applications from the field to the Northern Hemisphere. Agric. For. Meteorol. 228–229, 139–163.
Yang, X., Mustard, J.F., Tang, J., Xu, H., 2012. Regional-scale phenology modeling based on meteorological records and remote sensing observations. J. Geophys. Res.: Biogeosci. 117 (G3).
Yang, J., et al., 2013. The role of satellite remote sensing in climate change studies. Nat. Clim. Change 3 (10), 875.
Zeng, F., Collatz, G.J., Pinzon, J.E., Ivanoff, A., 2013. Evaluating and quantifying the climate-driven interannual variability in Global Inventory Modeling and Mapping Studies (GIMMS) Normalized Difference Vegetation Index (NDVI3g) at global scales. Remote Sens. 5 (8), 3918–3950.
Zhu, P., et al., 2017. Elevated atmospheric CO2 negatively impacts photosynthesis through radiative forcing and physiology-mediated climate feedback. Geophys. Res. Lett. 44 (4), 1956–1963.